JOURNAL OF AIRCRAFT
Vol. 42, No. 5, September–October 2005

Assessment of Comprehensive Analysis Calculation of Airloads on Helicopter Rotors

Hyeonsoo Yeo* and Wayne Johnson†
NASA Ames Research Center, Moffett Field, California 95035

Blade section normal force and pitching moment were investigated for six rotors operating at transition and high speeds: H-34 in flight and wind tunnel, SA 330 (research Puma), SA 349/2, UH-60A full-scale, and BO-105 model (Higher-Harmonic Acoustics Rotor Test I). The measured data from flight and wind-tunnel tests were compared with calculations obtained using the comprehensive analysis CAMRAD II. The calculations were made using two free-wake models: rolled up and multiple trailer with consolidation models. At transition speed, there is fair to good agreement for the blade section normal force between the test data and analysis for the H-34, research Puma, and SA 349/2 with the rolled-up wake. The calculated airloads differ significantly from the measurements for the UH-60A and BO-105. Better correlation is obtained for the UH-60A and BO-105 by using the multiple trailer with consolidation wake model. In the high-speed condition, the analysis shows generally good agreement with the research Puma flight data in both magnitude and phase. However, poor agreement is obtained for the other rotors examined. The analysis shows that the aerodynamic tip design (chord length and quarter-chord location) of the research Puma has an important influence on the phase correlation.

Nomenclature

C_T	=	rotor thrust coefficient
G	=	strength of trailed vorticity
M	=	Mach number
N_b	=	number of blades
R	=	blade radius
Re	=	Reynolds number
r	=	blade radial station
r_C	=	centroid of vorticity
r_G	=	moment (radius of gyration) of vorticity
α_{TPP}	=	tip path plane tilt angle, positive forward
Γ	=	bound circulation
μ	=	advance ratio
σ	=	solidity

Introduction

THE accurate prediction of rotor loads and vibration remains a difficult problem for helicopter design. Typically, helicopters encounter high vibration in two different speed regimes: transition and high speeds. The rotor blade aerodynamic environment at transition speed is characterized by blade–vortex interactions and at high speed by compressibility and negative loading on the advancing side. The ability to predict the rotor aerodynamic loading for these two flight regimes accurately is essential for the design of future rotorcraft.

For the past several decades, a number of flight and wind-tunnel tests have been conducted with pressure-instrumented blades, with the objective of improving the understanding of the nature of the aerodynamic loading acting on the rotor blade.[1–6] These extensive flight and wind-tunnel data sets provide a valuable resource that can be used to evaluate the accuracy and reliability of comprehensive codes in airload prediction and to develop better methodologies to simulate the rotor aerodynamic environment.

Received 15 June 2004; accepted for publication 3 October 2004.

*Research Scientist, MS 243-12, U.S. Army/NASA Rotorcraft Division, Aeroflightdynamics Directorate. Member AIAA.

†Research Scientist, MS 243-12, U.S. Army/NASA Rotorcraft Division. Member AIAA.

Analyses need to provide consistently good predictions for various rotors and flight conditions to be used for design work. For applications to advanced configurations, the analyses must be based as much as possible on first-principle aerodynamics, minimizing the use of empirical models. The first step to obtain better prediction is to understand the deficiencies of the current analyses. This can be achieved by comparing calculations with flight and wind-tunnel measurements for different rotors. Once the deficiencies are identified, effort can be made to improve the correlation.

The purpose of this study is threefold: 1) assess the accuracy and reliability of a comprehensive code in the calculation of airloads, 2) understand the similarities and differences in blade airloads among the measurements as well as calculations and investigate the deficiencies of the current analysis and key elements to improve the correlation, and 3) carry out calculations with various wake models and identify important wake parameters for the airload calculation.

The calculations were performed using the comprehensive analysis CAMRAD II (Ref. 7).

Test Data

Flight and wind-tunnel test cases from various rotors[1–6] have been carefully selected so that they represent similar test conditions. Figure 1 and Table 1 show the thrust and advance ratio considered and some of the rotor parameters. The thrust coefficient values range from $C_T/\sigma = 0.057$ to 0.079, and the advance ratios are in the range from $\mu = 0.129$ to 0.15 at transition and from $\mu = 0.361$ to 0.39 at high speed.

The flight[1] and wind-tunnel[2] tests of an H-34 helicopter have long been a standard for rotor airloads data. The section airloads data for the H-34 in flight were measured at seven radial stations ($r/R = 0.25, 0.40, 0.55, 0.75, 0.85, 0.9$, and 0.95) and were averaged over three consecutive revolutions. The section airloads data for the H-34 in a wind tunnel were measured at nine radial stations ($r/R = 0.25$, 0.40, 0.55, 0.75, 0.85, 0.9, 0.95, 0.97, and 0.99) and were averaged over 10 revolutions.

The research Puma (SA 330) data were obtained using a modified swept-tip blade rather than the standard rectangular Puma blade.[3] Absolute pressures were measured at $r/R = 0.92$, 0.95, and 0.978. A single revolution of data was taken for each test point; therefore, there is no averaging of data.

The SA 349/2 flight data were obtained from an upgraded Gazelle helicopter with three research Grande Vitesse blades.[4] Absolute pressures were measured at $r/R = 0.75$, 0.88, and 0.97. Data from each of the pressure transducers were acquired over a period of six consecutive rotor revolutions and then averaged.

Table 1 Rotor parameters and operating conditions

Parameter	H-34	H-34	SA 330	SA 349/2	UH-60A	BO-105
Configuration	Articulated	Articulated	Articulated	Articulated	Articulated	Hingeless
N_b	4	4	4	3	4	4
σ	0.0622	0.0622	0.091	0.0627	0.0826	0.077
Test	Flight	Wind tunnel	Flight	Flight	Flight	Wind tunnel
Radius, in.	336.0	336.0	296.7	206.7	322.0	78.7
Scale	Full-scale	Full-scale	Full-scale	Full-scale	Full-scale	Model-scale
Low speed						
C_T/σ	0.075		0.070	0.065	0.079	0.057
μ	0.129		0.141	0.140	0.149	0.150
α_{TPP}, deg	4.1		1.3	1.2	0.8	−4.2
$M_{90,tip}$	0.628		0.672	0.719	0.740	0.735
High speed						
C_T/σ		0.060	0.070	0.071	0.079	
μ		0.390	0.362	0.361	0.368	
α_{TPP}, deg		6.0	7.5	7.5	8.0	
$M_{90,tip}$		0.803	0.803	0.872	0.878	

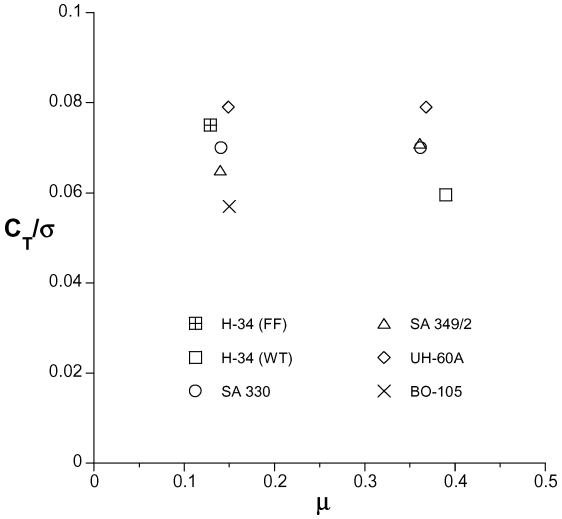

Fig. 1 Rotor thrust coefficient and advance ratio of test data examined.

Test data with the UH-60A were obtained from the NASA/Army UH-60A Airloads Program.[5] Absolute pressures were measured at $r/R = 0.225$, 0.40, 0.55, 0.675, 0.775, 0.865, 0.92, 0.965, and 0.99. For this study, a single revolution of data was taken for each test point.

The BO-105 data were obtained from the Higher-Harmonic Acoustics Rotor Test (HART-I) Program using a 40% Mach-scaled hingeless BO-105 main rotor blade.[6] The objective of the test was to demonstrate the reduction of blade–vortex interactions (BVI) noise in the descending flights using higher-harmonic controls. The data set used for the current study is a baseline case without higher-harmonic pitch control inputs. A shaft angle for this condition was 5.3-deg aft (4.2-deg aft when corrected for tunnel wall effect). Absolute pressures were measured at $r/R = 0.75$, 0.87, and 0.97. The HART-I data were averaged over 64 revolutions.

Figure 2 shows the blade planforms for the five rotors, along with the location of the airfoils used and the pressure measurements. Figure 3 shows the blade twist distributions. Most of the rotor blades have about −8 deg of twist, whereas the UH-60A has about −16-deg twist, and its distribution is nonlinear near the tip.

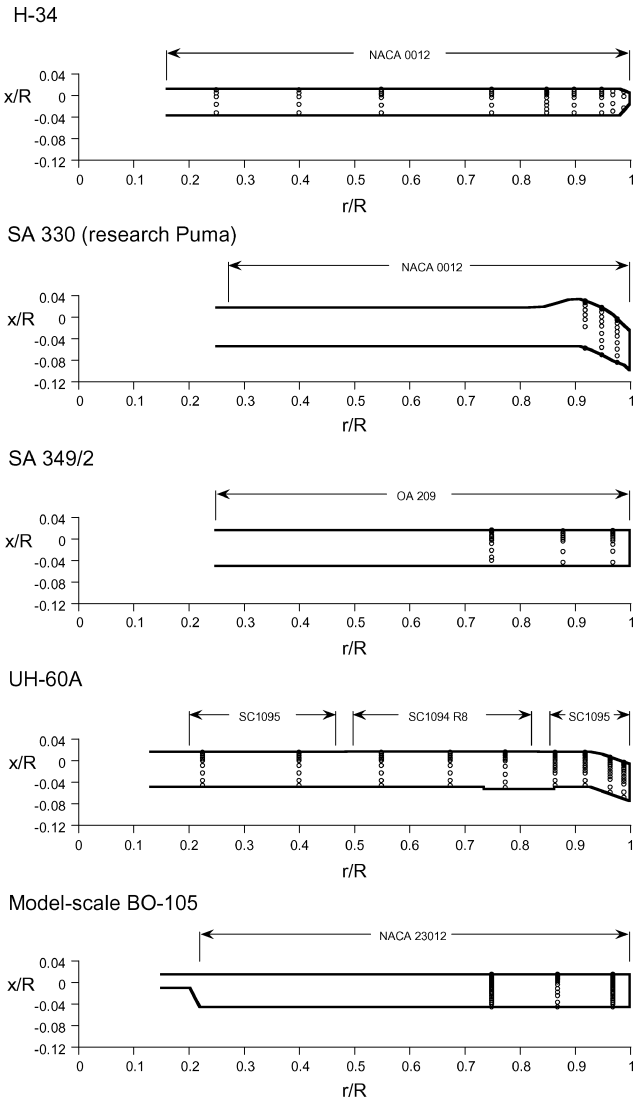

Fig. 2 Blade planforms: ○, pressure measurements.

CAMRAD II Modeling

The H-34 in flight and wind tunnel, research Puma and UH-60A Black Hawk in flight, and model-scale BO-105 in wind tunnel were modeled in CAMRAD II as isolated rotors. The trim solution for the H-34 in flight and wind tunnel and the research Puma in flight were solved for the controls that produced rotor thrust and first harmonic flapping to match the measured values, with the rotor shaft angle of attack fixed at the measured values. The trim solution for the UH-60A in flight and BO-105 in wind tunnel were solved for the controls that produced rotor thrust and shaft pitch and roll moments to match the measured values, with the rotor shaft angle of attack fixed at the measured values.

The SA 349/2 in flight was modeled as a complete aircraft, with the Fenestron tail rotor replaced by an auxiliary antitorque force. The trim solution for the SA 349/2 in flight was solved for the controls and aircraft attitudes that produced zero total force and moment on the aircraft, with zero sideslip angle.

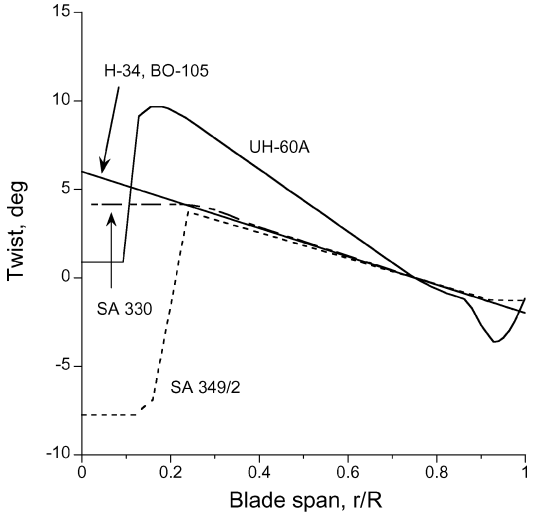

Fig. 3 Blade twist angle.

Aerodynamic and Wake Model

The CAMRAD II aerodynamic model for the rotor blade is based on lifting-line theory by the use of steady two-dimensional airfoil characteristics and a vortex wake model. The rotor blade modeling problem of lifting-line theory is unsteady, compressible, viscous flow about an infinite aspect-ratio wing, in a uniform flow consisting of the yawed freestream and the wake-induced velocity. This problem is modeled as two-dimensional, steady, compressible, viscous flow (airfoil tables), plus corrections. The corrections in particular account for swept and yawed flow, spanwise drag, and attached flow unsteady loads.

The wake problem of lifting line theory is an incompressible vortex wake behind the lifting line, with distorted geometry and rollup. The lifting line (bound vortex) is at the quarter-chord (an approximation for the quadrupole line of second-order loading), and the three components of wake-induced velocity are evaluated at collocation points at the three-quarter-chord (an approximation for the linearly varying induced velocity introduced by second-order wake). This model is generally second-order accurate for section lift, which significantly improves the calculation of blade–vortex interaction loading, but is less accurate for section moments.

The wake analysis calculates the rotor nonuniform induced velocity using free-wake geometry. The concentrated tip vortices are the key features of the rotor wake, important for performance, airloads, structural loads, vibration, and noise calculations. The formation of the tip vortices is modeled in CAMRAD II, not calculated from first principles. Two cases are examined here: a rolled-up model and a multiple trailer with consolidation model. Because of its simplicity and efficiency, the rolled-up model has long been used for helicopter rotors. The multiple-trailer model has also been available, and with the consolidation feature has been applied recently with success to tiltrotor airloads calculations.[8]

The rolled-up wake model is based on the assumption that a tip vortex forms at the outboard blade tip. The bound circulation can have the same sign all along the blade span, or there may be two bound circulation peaks (inboard and outboard peaks of opposite sign). These are the single-peak and dual-peak cases. The rolled-up wake is constructed from the magnitude and position of the peak bound circulation. For the single-peak case, the maximum bound circulation is $\Gamma_{\max}$. In the far wake (where the rollup process is complete), there is a tip vortex with strength equal to $\Gamma_{\max}$ at the time that the wake element was created; there is corresponding negative trailed vorticity with total strength $-\Gamma_{\max}$ in an inboard sheet. The tip vortex is modeled as a line segment with this strength and a small core radius. Any error in the assumed strength (because the vortex is partially or over rolled up) is compensated for by the value used for the core radius. The detailed structure of the inboard vortex sheet is not calculated, and so a single sheet element with trailed and shed vorticity is used. For the dual-peak case, the bound circulation can be positive over part of the blade span, but negative at the blade tip. In this case, the tip vortex consists of the trailed vorticity from the outboard peak to the tip; hence, it has strength equal to the outboard peak bound circulation. The inboard wake sheet now has both positive and negative trailed vorticity, divided at the radial station corresponding to the inboard circulation peak. The trailed vorticity between the two circulation peaks might also roll up. For the current study, the single-peak model was used for the low-speed conditions, and the dual-peak model was used for the high-speed conditions.

The multiple-trailer model has the far wake trailed vorticity divided into several spanwise panels, to provide more detailed structure for the inboard vorticity, with consolidation of trailed lines in the wake geometry to model the rollup process. This model has a discrete trailed vortex line emanating from each of the aerodynamic panel edges. The calculation of the free-wake geometry includes the distortion of all of these trailed lines. With multiple far wake trailed vorticity panels, the trailed lines at the aerodynamic panel edges can be consolidated into rolled-up lines, using the trailed vorticity moment to scale the rate of rollup. The trailed vorticity is partitioned into sets of adjacent lines that have the same sign (bound circulation increasing or decreasing). For each set, the total strength G, centroid r_C, and moment (radius of gyration) r_G of the trailed vorticity set are calculated:

$$G = \int \left(\frac{-\partial \Gamma}{\partial r} \right) \mathrm{d}r$$

$$G r_C = \int \left(\frac{-\partial \Gamma}{\partial r} \right) r \, \mathrm{d}r$$

$$G r_G^2 = \int \left(\frac{-\partial \Gamma}{\partial r} \right) (r - r_C)^2 \, \mathrm{d}r$$

It is assumed that all of the vorticity in each set eventually rolls up into a single vortex, located at the centroid of the original vorticity distribution. The characteristic time (r_G^2/Γ) is taken as a measure of the rate of consolidation

Results and Discussion

The calculated blade section normal force and pitching moment were compared with the flight and wind-tunnel measurements. The calculations have been conducted with the identical analysis options for all rotors. The azimuthal step size was 15 deg for the aerodynamic and structural-dynamic calculations. A constant vortex core radius of 20% chord ($0.2c$) was used for the rolled-up wake model. The consolidation model used a compression form, with linear dependence of the rollup fraction as wake age. The vortex core radius had a constant value of 10% mean chord near the blade tip (from $80\%R$ to $100\%R$) and 100% mean chord at inboard (root cutout to $80\%R$). For all cases, an elastic blade model was used to calculate the airloads.

Airloads Correlation at Low Speed

Figure 4 shows nondimensionalized blade section normal force near 90% radial station of the H-34, research Puma, SA 349/2, UH-60A Black Hawk, and BO-105 rotors at an advance ratio of 0.129, 0.141, 0.14, 0.149, and 0.15, respectively. At low speed in the transition regime, the airloads are mainly determined by the interaction between the blades and the vortices trailed from the preceding blades.[9] All of the flight test data show a sharp "down–up" impulse on the advancing blade and an opposite impulse on the retreating blade near the blade tip.

A free wake is important for the prediction of airloads in low-speed flight. The analysis used two wake models: a rolled-up and a multiple-trailer wake with consolidation. The multiple-trailer wake with consolidation, which showed better airload correlation for the UH-60A (Ref. 10) and BO-105 (Ref. 11) rotors, was applied to five different rotors to assess the general utility of this wake model.

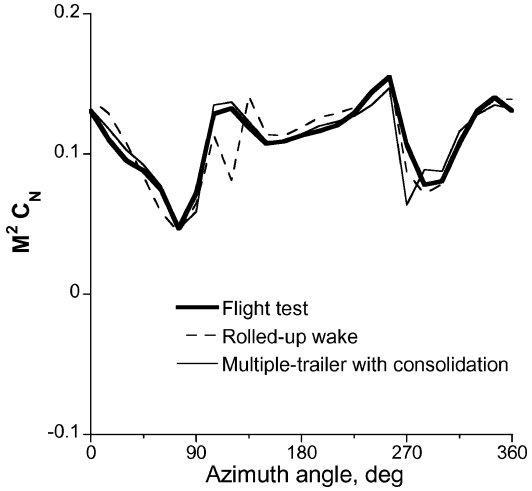

a) H-34 at $\mu = 0.129$, $r/R = 0.90$

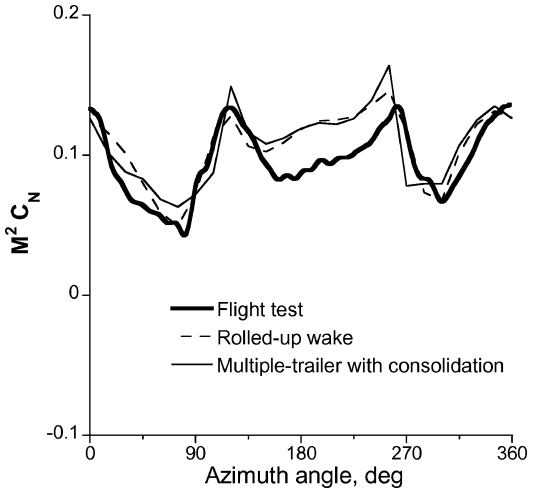

c) SA 349/2 at $\mu = 0.14$, $r/R = 0.88$

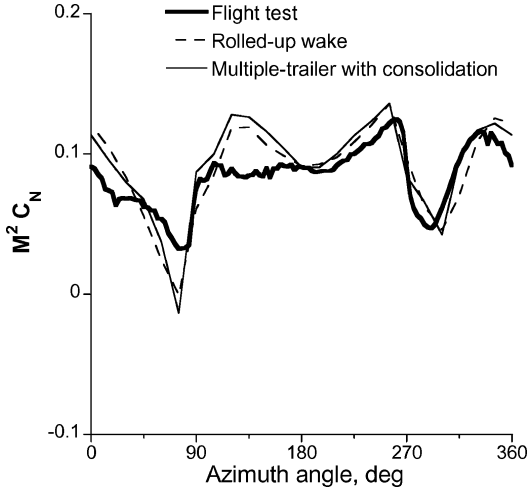

b) SA 330 at $\mu = 0.141$, $r/R = 0.92$

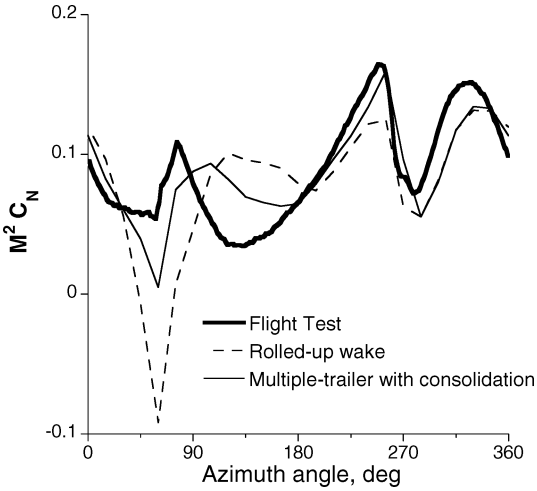

d) UH-60A at $\mu = 0.149$, $r/R = 0.92$

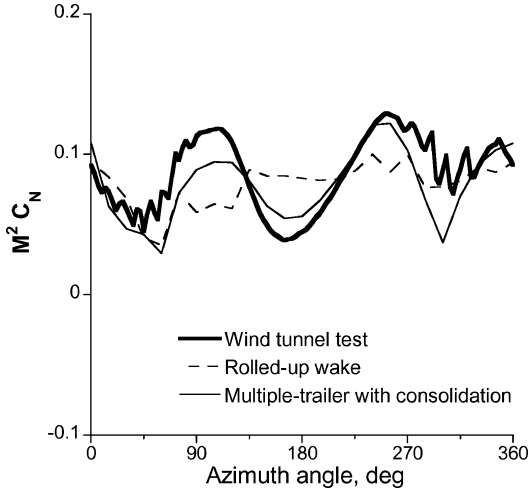

e) BO-105 at $\mu = 0.15$, $r/R = 0.87$

Fig. 4 Calculated and measured blade normal force at low speed near $r/R = 0.9$.

The analysis with the rolled-up wake model captured the rapid changes of airloads reasonably well for the H-34, research Puma, and SA 349/2. The calculated airloads differed significantly from the measurements for the UH-60A and BO-105. The rolled-up wake model significantly overpredicted the magnitude of the down–up impulse on the advancing side for the UH-60A and underpredicted that for the BO-105.

Better correlation was obtained for the UH-60A and BO-105 by using a free-wake geometry calculation method that combines the multiple-trailer wake with a simulation of the tip vortex formation process (consolidation). However, the influence of the multiple trailer with consolidation model was different for the two rotors. For the UH-60A, the multiple trailer with consolidation model reduced BVI compared to the rolled-up wake on the advancing side and, thus, improved the correlation. For the BO-105, the multiple trailer with consolidation model increased BVI on the advancing side and, thus, improved the correlation. The correlation with the multiple-trailer wake was better than with the rolled-up wake on

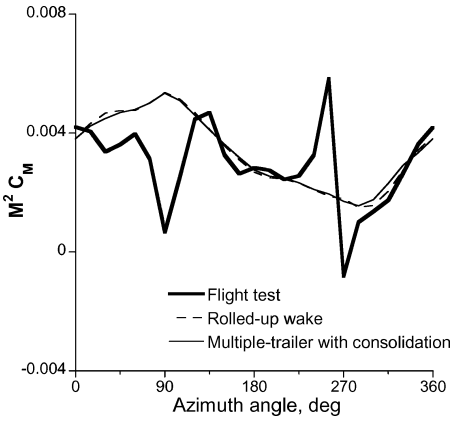

a) H-34 at $\mu = 0.129$, $r/R = 0.90$

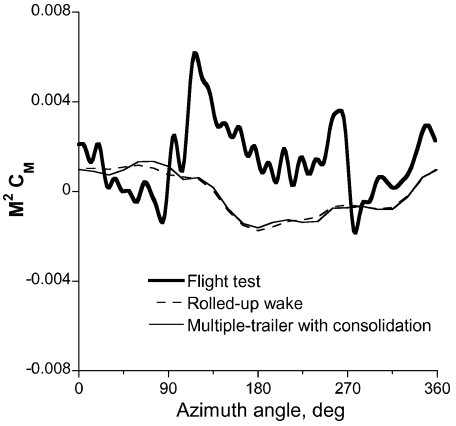

c) SA 349/2 at $\mu = 0.14$, $r/R = 0.88$

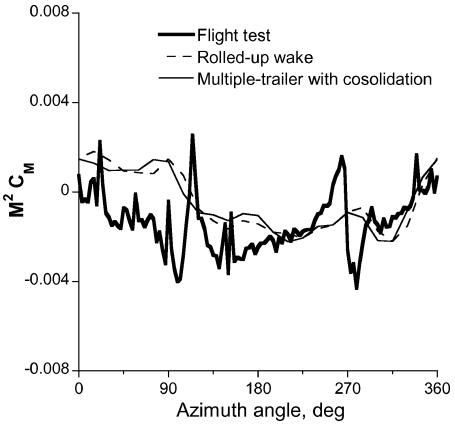

b) SA 330 at $\mu = 0.141$, $r/R = 0.92$

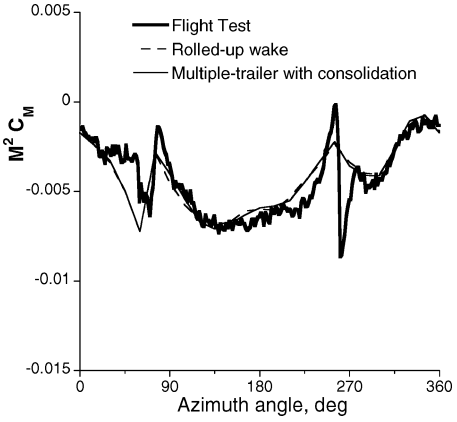

d) UH-60A at $\mu = 0.149$, $r/R = 0.92$

Fig. 5 Calculated and measured blade pitching moment force at low speed near $r/R = 0.9$.

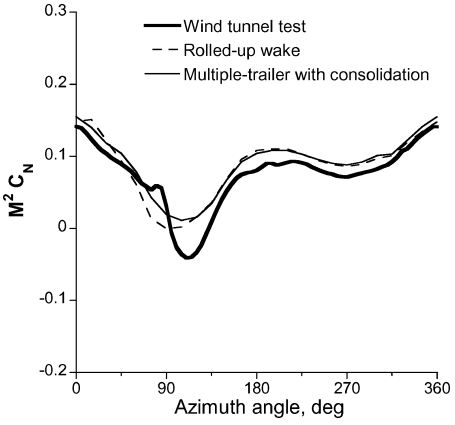

a) H-34 at $\mu = 0.39$, $r/R = 0.90$

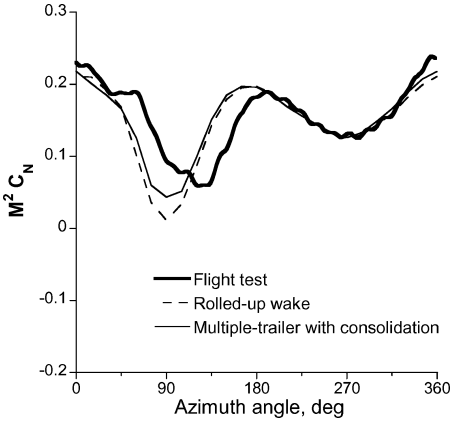

c) SA 349/2 at $\mu = 0.361$, $r/R = 0.88$

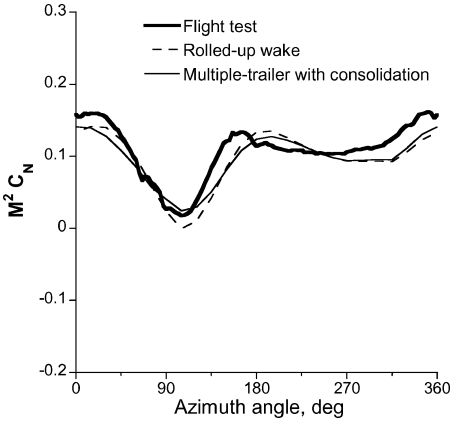

b) SA 330 at $\mu = 0.362$, $r/R = 0.92$

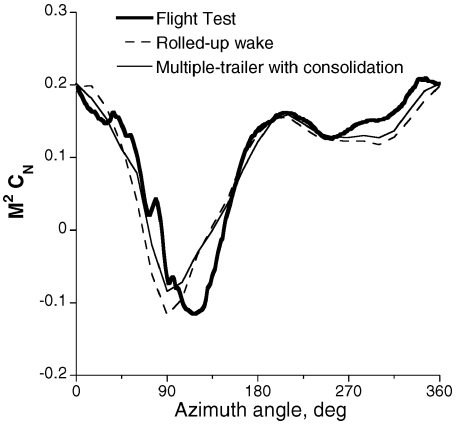

d) UH-60A at $\mu = 0.368$, $r/R = 0.92$

Fig. 6 Calculated and measured blade normal force at high speed near $r/R = 0.9$.

the front of the rotor disk, as well for the UH-60A and BO-105. For the other rotors, the multiple trailer with consolidation model had less influence on the accuracy of the prediction of the normal force. There was a small magnitude change on the advancing and retreating sides, but, in general, the phase was not changed.

Note that the high-frequency loading observed in the BO-105 test data is the source of BVI noise. A smaller time step would be required to capture the high-frequency content. However, the scope of the present study is loads and vibration; thus, the 15-deg time step was consistently used.

Figure 5 shows blade section pitching moment correlation. The measured pitching moment values for the BO-105 have not yet been published for the HART-I; thus, the comparison with the analysis was not included in this paper. The measured pitching moment data show more high-frequency content than the normal force data. In general, the correlation is poor with either of the wake models.

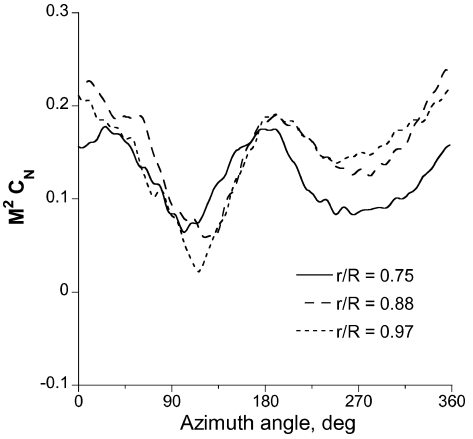

Fig. 7 Measured normal force for the SA 349/2 at high speed.

Airloads Correlation at High Speed

Figure 6 shows blade section normal force of the H-34, research Puma, SA 349/2, and UH-60A Black Hawk rotors at an advance ratio of 0.39, 0.362, 0.361, and 0.368, respectively. At high speed, the interaction between the blade and wake diminishes as the rotor disk is tilted further forward and the tip vortices are convected more quickly away from the rotor disk. The airloads on the blade tip region are characterized by negative lift at the end of the first quadrant and the beginning of the second quadrant.[9] This negative loading occurs on the H-34, research Puma, and UH-60A Black Hawk rotors. The SA 349/2 flight-test data, as shown in Fig. 7, do not show the negative loading, although the flight condition (C_T/σ and μ) is similar to the other rotor tests.

Comparison of calculation with the research Puma flight-data shows, in general, good agreement with the measurements in both magnitude and phase. However, good agreement is not obtained for the other rotors examined. Although the amplitude shows fair to good correlation for some of the rotors, there is about a 20–30 deg phase difference. The multiple trailer with consolidation model has a small influence on the prediction of normal force at high speed. The phase difference between the test data and analysis does not appear to come from the wake modeling.

Figure 8 shows blade section pitching moment correlation. The correlation for the H-34 is fair to good. In general, the correlation is poor for the other rotors examined.

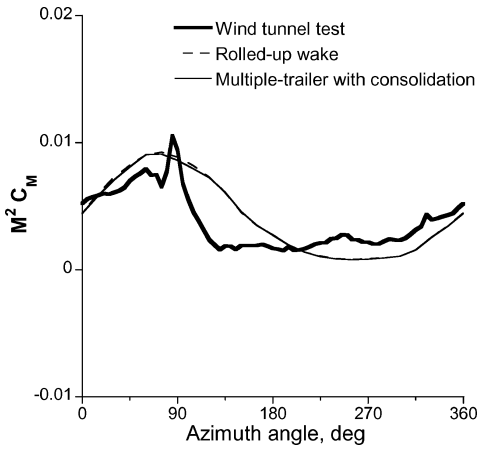

a) H-34 at $\mu = 0.39$, $r/R = 0.90$

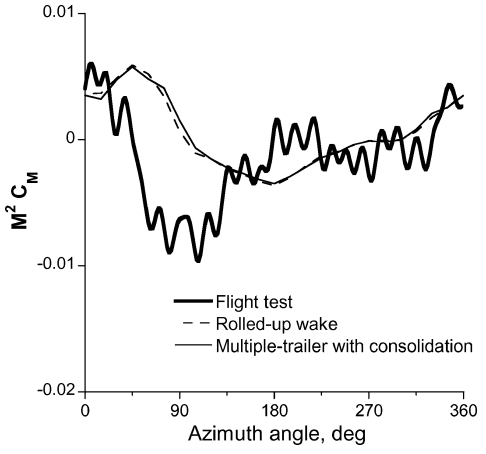

c) SA 349/2 at $\mu = 0.361$, $r/R = 0.88$

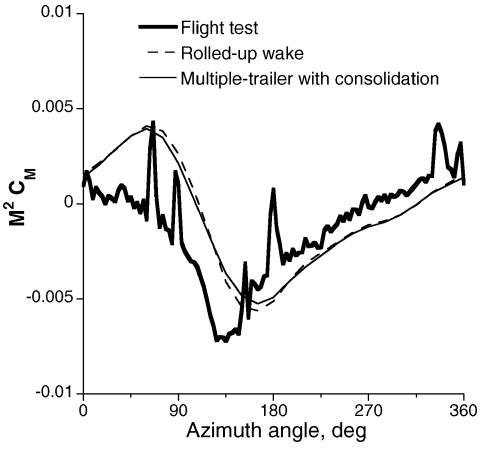

b) SA 330 at $\mu = 0.362$, $r/R = 0.92$

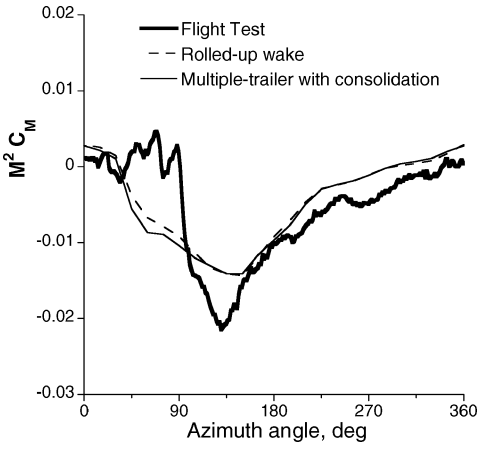

d) UH-60A at $\mu = 0.368$, $r/R = 0.92$

Fig. 8 Calculated and measured blade pitching moment at high speed near $r/R = 0.9$.

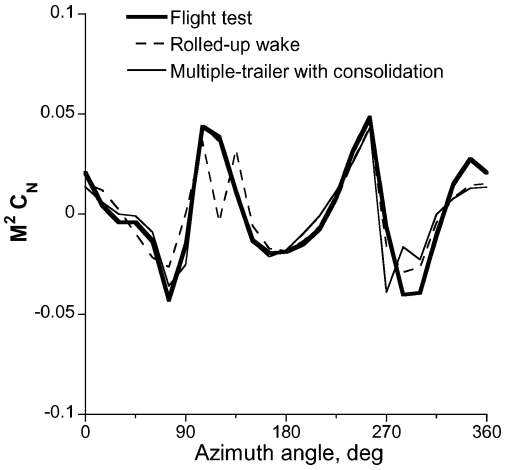

a) H-34 at $\mu = 0.129$, $r/R = 0.90$

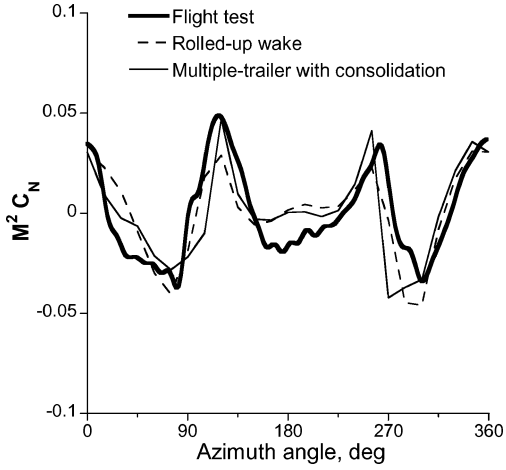

c) SA 349/2 at $\mu = 0.14$, $r/R = 0.88$

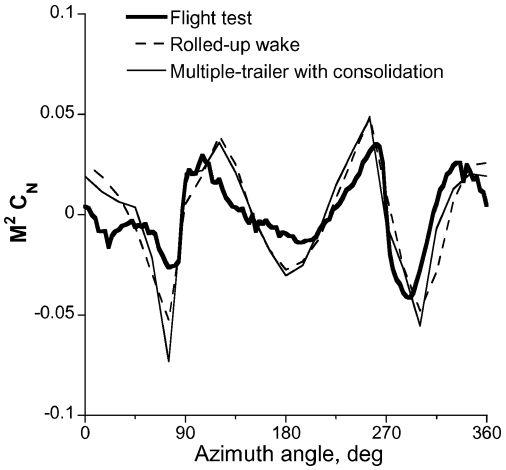

b) SA 330 at $\mu = 0.141$, $r/R = 0.92$

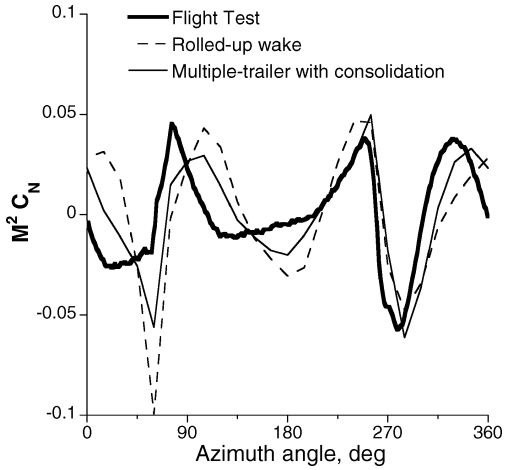

d) UH-60A at $\mu = 0.149$, $r/R = 0.92$

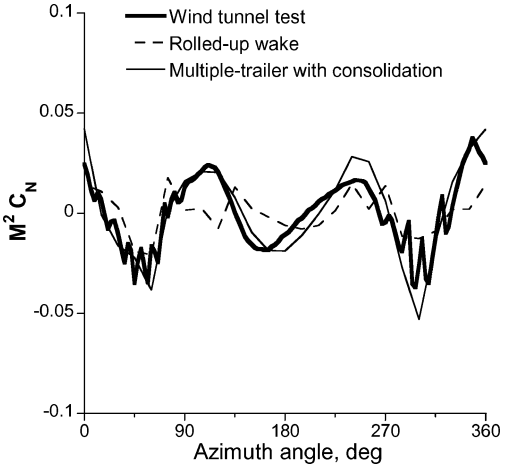

e) BO-105 at $\mu = 0.15$, $r/R = 0.87$

Fig. 9 Calculated and measured blade vibratory normal force at low speed near $r/R = 0.9$.

Vibratory Airloads at Low and High Speeds

Figure 9 shows the blade vibratory normal force at low speed. Steady, 1/revolution, and 2/revolution harmonics have been removed from the test data and analyses for the four-bladed rotors (H-34, research Puma, UH-60A, and BO-105). Steady and 1/revolution harmonics have been removed for the three-bladed SA 349/2. The harmonics retained are the vibratory loads that are transmitted through the shaft to the fuselage and produce vibration of multiples of N_b per revolution. All of the measured vibratory airloads are quite similar. The 3/revolution harmonic is dominant for both three- and four-bladed rotors.

Both the rolled-up and multiple trailer with consolidation wake models show fair to good correlation for the H-34, research Puma, and SA 349/2. A larger difference between the two wake models appeared for the UH-60A and BO-105. The multiple trailer with consolidation model showed better correlation than with the rolled-up wake, especially on the advancing side and the front of the rotor disk.

Figure 10 shows the blade vibratory normal force at high speed. The higher harmonic airloads show a sharp up–down impulse in the first and second quadrants. At low speed, the vibratory loads were dominated by 3/revolution harmonic regardless of the number of

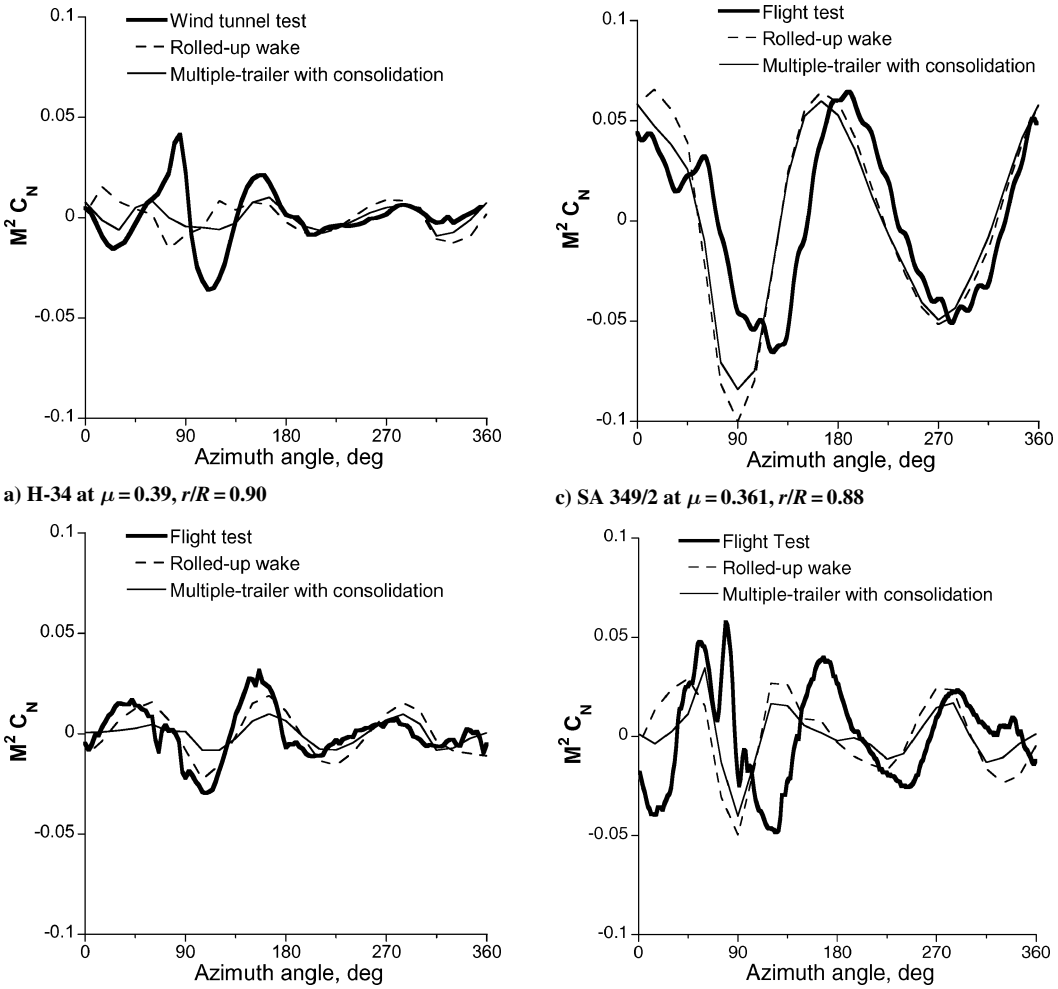

a) H-34 at $\mu = 0.39$, $r/R = 0.90$

c) SA 349/2 at $\mu = 0.361$, $r/R = 0.88$

b) SA 330 at $\mu = 0.362$, $r/R = 0.92$

d) UH-60A at $\mu = 0.368$, $r/R = 0.92$

Fig. 10 Calculated and measured blade vibratory normal force at high speed near $r/R = 0.9$.

blades. However, there are many differences among the measurements at high speed. A strong 5/revolution harmonic is observed for the H-34, and a 2/revolution harmonic is dominant for the SA 349/2 rotor. The correlation, in general, is poor to fair. For the H-34, there was a significant difference between the data and the analysis for both magnitude and phase. Better correlation was observed for the research Puma compared to the other rotors. For the UH-60A, the calculation shows nearly an opposite phase on the advancing side.

Comparison of Blade Oscillatory Normal Force

Figures 11 and 12 compare the blade oscillatory normal force near $r/R = 0.9$, where the steady airloads have been removed from the test data and calculations. In Figs. 11 and 12, the test data and the calculated airloads are grouped separately.

Figure 11 shows the blade oscillatory normal force at low speed. Steady, level flight-test data (H-34, research Puma, SA 349/2, and UH-60A) show that the minimum peak on the advancing side appears at 58–82 deg azimuth angle, and the minimum peak on the retreating side appears at 280–300 deg azimuth angle. For the BO-105 in the descending condition, the minimum peaks appear around 45- and 310-deg azimuth angle. The normal force values on the front of the rotor disk are close to zero for the H-34, research Puma, and SA 349/2. However, strong negative values are observed for the UH-60A and BO-105 rotors.

The analysis with the rolled-up wake shows similar phase for the H-34, research Puma, and SA 349/2: the minimum peak on the advancing side at 75 deg and on the retreating side at 285–300 deg. The normal force values on the front of the rotor disk are close to zero with the rolled-up wake model for all of the rotors. The multiple-trailer wake captures strong negative values on the front of the rotor disk observed for the UH-60A and BO-105 rotors.

Figure 12 shows the blade oscillatory normal force at high speed. There are many similarities in the measured normal force among the H-34, research Puma, and SA 349/2 rotors. The UH-60A data show a stronger negative peak, probably because the UH-60A blade has more twist than the other rotor blades as shown in Fig. 3. The negative peak appears between 108 deg for the research Puma and 122 deg for the UH-60A. However, the analysis shows that the minimum normal force appears at the 90-deg azimuth angle regardless of the rotor except for the research Puma, where the minimum normal force appears at 105 deg.

Parametric Study of High-Speed Airload Calculation

The calculation shows good phase correlation at high speed for the research Puma, whereas the same analysis cannot predict the correct phase for the other rotors examined. It is important to understand why the same analysis shows good correlation for one rotor but not the others. This can be examined using the research Puma and UH-60A rotors because the two articulated rotors have a similar size and both have swept tips.

There are many differences between the two rotors, structurally and aerodynamically. The research Puma has the NACA 0012 airfoil along the span, whereas the UH-60A blade uses two airfoils, the SC1095 and SC1094 R8. Another significant difference between the two rotors is the blade twist, as shown in Fig. 3. The Puma has about -8 deg of twist, whereas the UH-60A has about a -16-deg twist, and its distribution is nonlinear near the tip. Figure 13 shows that the two blades have almost same chord length at the straight

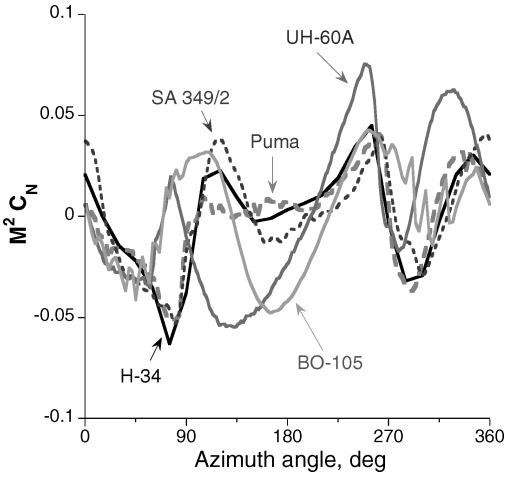

a) Test data

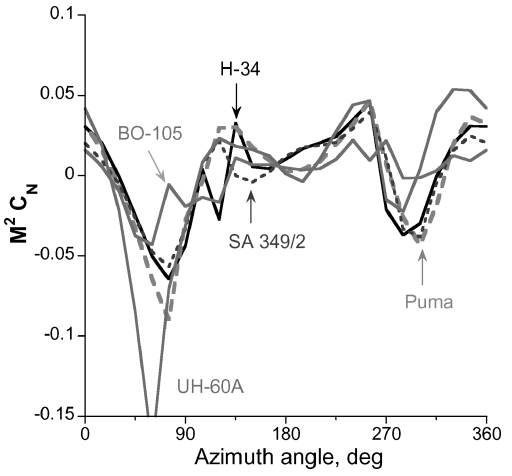

b) Rolled-up wake

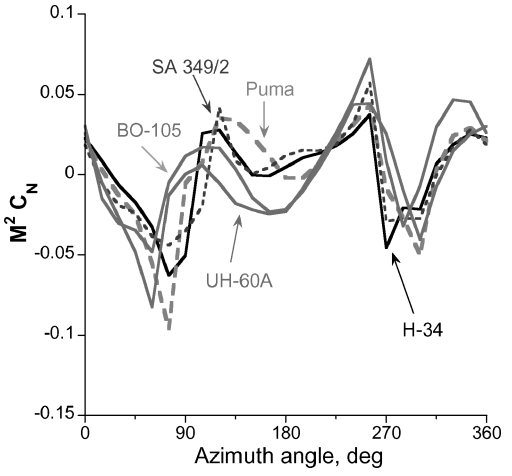

c) Multiple trailer with consolidation

Fig. 11 Comparison of blade oscillatory normal force at low speed near $r/R = 0.9$.

portion of a blade, but the chord length is increased for the Puma near $r/R = 0.9$. The quarter-chord of the Puma is forward of the quarter-chord of the UH-60A near $r/R = 0.9$ and then moves aft of the quarter-chord of the UH-60A near the tip. There is also a slight difference in flight and trim condition.

The parameters investigated in this study are: airfoil, twist, structural tip design (elastic axis and center of gravity location), aerodynamic tip design (chord length and quarter-chord location), and trim (flight) condition. The effects of those parameters on the prediction

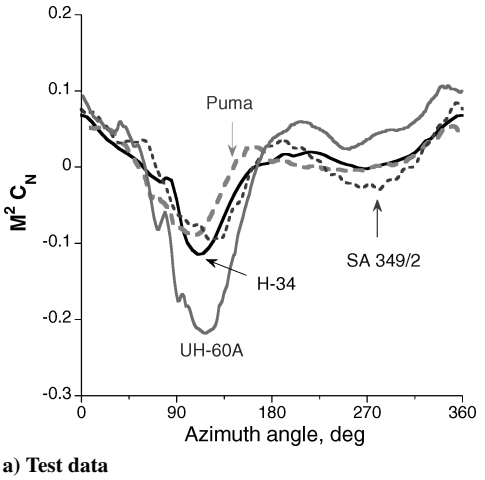

a) Test data

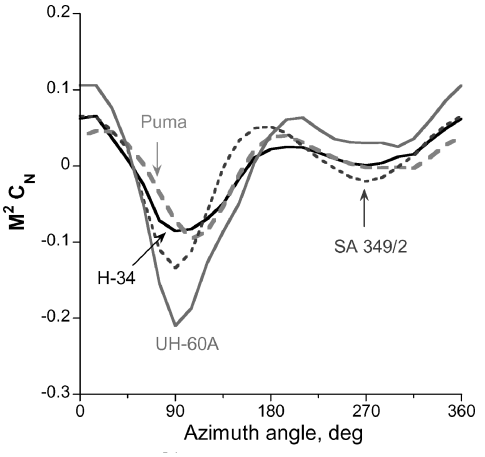

b) Rolled-up wake

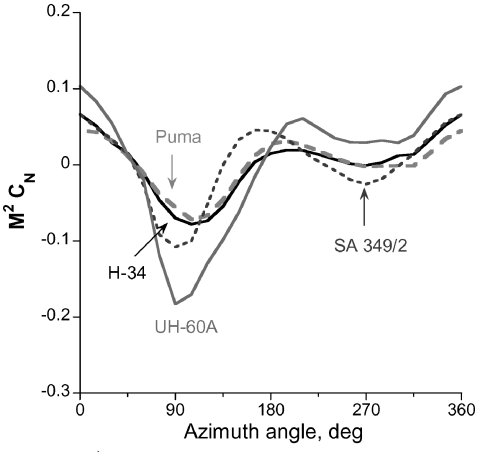

c) Multiple trailer with consolidation

Fig. 12 Comparison of blade oscillatory normal force at high speed near $r/R = 0.9$.

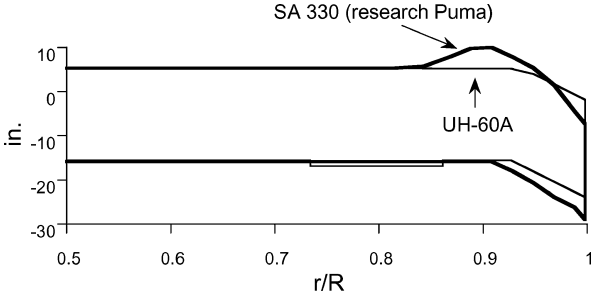

Fig. 13 Comparison of blade tip geometry between research Puma and UH-60A.

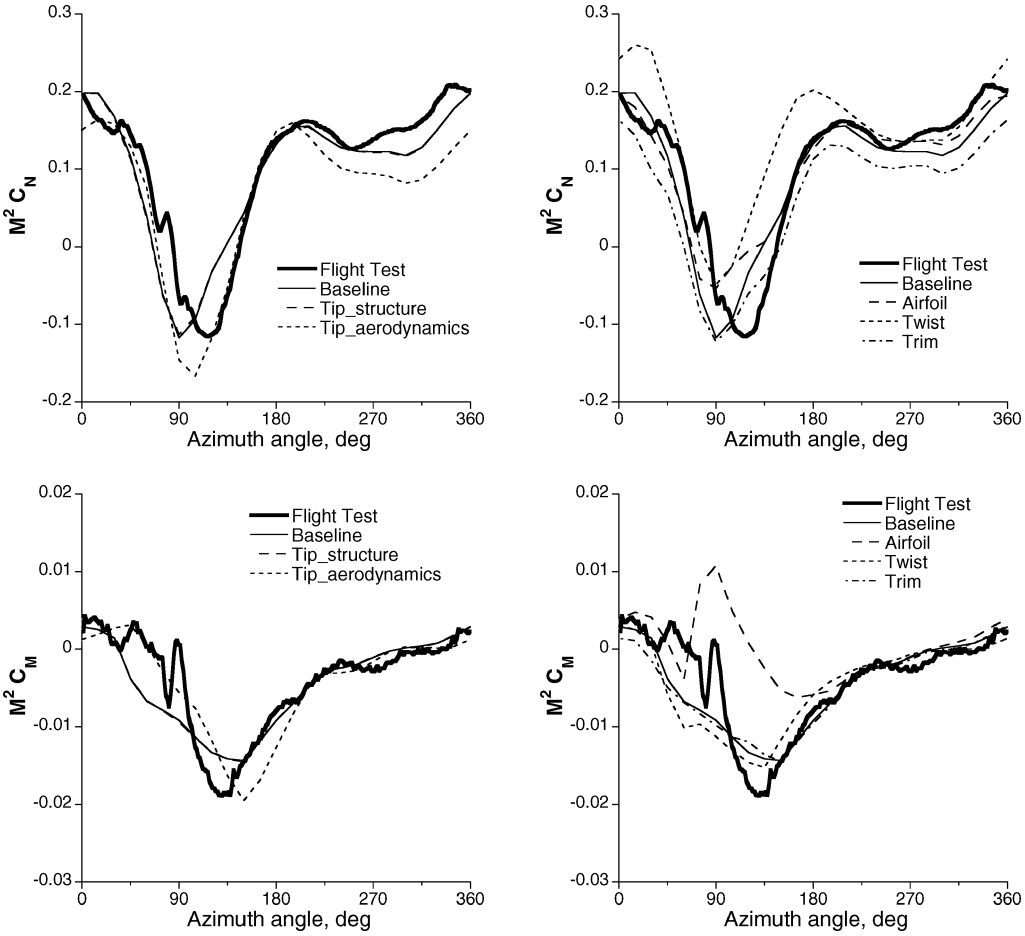

Fig. 14 Blade airloads at $r/R = 0.92$ for UH-60A at $\mu = 0.368$ using the Puma parameters.

of blade airloads were examined by replacing the UH-60A quantities with the equivalent research Puma quantities. For example, the SC1095 and SC1094 R8 airfoils were replaced with the NACA 0012 airfoil to understand the influence of airfoil on the prediction of blade airloads.

Figure 14 shows the blade normal force and pitching moment of the UH-60A at $r/R = 0.92$. The structural tip design and trim condition have a small influence on the normal force prediction. The airfoil and twist change the magnitude, but not the phase. The only parameter that changed the phase of the normal force is the aerodynamic tip design (chord length and quarter-chord location). The negative peak appears at 105-deg azimuth angle by using the chord length and quarter-chord of the Puma. However, the quarter-chord or chord length alone did not change the phase.

Most of the parameters have a small influence on the pitching moment prediction. The airfoil change from the cambered to symmetric produces less negative pitching moment. The aerodynamic tip design shows better pitching moment correlation. This additional pitching moment appears to shift the normal force phase by 15 deg.

Conclusions

Blade section normal force and pitching moment were investigated for various rotors operating at transition and high speeds: H-34 in flight and wind tunnel, SA 330 (research Puma), SA 349/2, UH-60A full-scale, and BO-105 model (HART-I). The H-34, research Puma, SA 349/2, and UH-60A data represent steady, level flight conditions and the BO-105 data represent descending flight condition. Measured data from flight and wind-tunnel tests were compared with calculations obtained using the comprehensive analysis CAMRAD II.

From this study the following conclusions were obtained for low speed:

1) All of the measured blade section normal force data show a sharp down–up impulse on the advancing blade and an opposite impulse on the retreating blade. All of the measured vibratory normal forces are quite similar at low speed. The 3/revolution harmonic is dominant for both three-bladed and four-bladed rotors.

2) The analysis with a rolled-up wake model captures the rapid changes of airloads reasonably well for the H-34, research Puma, and SA 349/2. The calculated airloads differ significantly from the measurements for the UH-60A and BO-105.

3) Better correlation is obtained for the UH-60A and BO-105 by using a free-wake geometry calculation method that combines the multiple-trailer wake with a simulation of the tip vortex formation process (consolidation).

4) The measured pitching moment data show more high-frequency content than the normal force data. In general, the correlation is poor with either of the wake models.

The following conclusions were obtained for high speed: 1) In high-speed flight, the airloads on the blade tip region are characterized by negative lift at the end of the first quadrant and the beginning of the second quadrant. This negative loading occurs on the H-34, research Puma, and UH-60A Black Hawk rotors. The SA 349/2 flight-test data do not show the negative loading, although the flight condition (C_T/σ and μ) is similar to the other rotor tests.

2) The comparison of the calculated blade section normal force with the research Puma flight data shows, in general, good agreement with the measurements in both magnitude and phase. However, poor agreement is obtained for the other rotors examined. There is about a 20–30 deg phase difference.

3) The correlation of the pitching moment for the H-34 is fair to good. In general, the correlation is poor for the other rotors examined.

4) The parametric study shows that the aerodynamic tip design (quarter-chord location and chord length) of the research Puma has an important influence on the phase correlation.

References

[1]Scheiman, J., "A Tabulation of Helicopter Rotor-Blade Differential Pressures, Stresses, and Motions as Measured in Flight," NASA TM X-952, March 1964.

[2]Rabbott, J. P., Jr., Lizak, A. A., and Paglino, V. M., "A Presentation of Measured and Calculated Full-Scale Rotor Blade Aerodynamic and Structural Loads," USAAVLABS TR 66-31, 1966.

[3]Bousman, W. G., Young, C., Gilbert, N. E., Strawn, R. C., Miller, J. V., Maier, T. H., Costes, M., and Beaumier, P., "A Comparison of Lifting-Line and CFD Methods with Flight Test Data from a Research Puma Helicopter," NASA TM 110421, Oct. 1996.

[4]Heffernan, R. M., and Gaubert, M., "Structural and Aerodynamic Loads and Performance Measurements of an SA349/2 Helicopter with an Advanced Geometry Rotor," NASA TM 88370, Nov. 1986.

[5]Kufeld, R. M., Balough, D. L., Cross, J. L., Studebaker, K. F., Jennison, C. D., and Bousman, W. G., "Flight Testing of the UH-60A Airloads Aircraft," *American Helicopter Society 50th Annual Forum*, American Helicopter Society, May 1994.

[6]Splettstoesser, W. R., Heller, H., Mercker, E., Preisser, J. S., and Yu, Y. H., "The HART Programme, A Quadrilateral Cooperative Research Effort," *American Helicopter Society 51st Annual Forum*, American Helicopter Society, May 1995.

[7]Johnson, W., "Technology Drivers in the Development of CAMRAD II," *American Helicopter Society 51st Annual Forum*, American Helicopter Society, Jan. 1994.

[8]Johnson, W., "Influence of Wake Models on Calculated Tiltrotor Aerodynamics," *American Helicopter Society Aeromechanics Specialist Meeting*, American Helicopter Society, Jan. 2002.

[9]Hooper, W. E., "The Vibratory Airloads of Helicopter Rotors," *Vertica*, Vol. 8, No. 2, 1984, pp. 73–92.

[10]Yeo, H., and Shinoda, P. M., "Investigation of Rotor Loads and Vibration at Transition Speed," *American Helicopter Society 58th Annual Forum*, American Helicopter Society, June 2002.

[11]Lim, J. W., and Yu, Y. H., "Prediction of Blade–Vortex Induced Airloads with a Multiple-Trailer Free Wake Model," *American Helicopter Society International Meeting on Advanced Rotorcraft Technology and Life Saving Activities*, American Helicopter Society, Nov. 2002.